Competing interests None.

Patient consent Obtained.

Ethics approval Ethics approval was provided by Kyoto Prefectural University of Medicine.

Provenance and peer review Not commissioned; externally peer reviewed.

REFERENCES

1 Mooren A. *Ulcus rodens (in German) Ophthalmiatrische Beobachtungen*. Berlin: Hirschwald, 1867:107–10.
2 Zaidman GW, Mondino BJ. Mooren's ulcer. In: Krachmer JH, Mannis MJ Holland EJ, eds. *Cornea*. St Louis, Missouri: Mosby, 1997:1397–401.
3 Murray PI, Rahi HS. Pathogenesis of Mooren's ulcer: some new concepts. *Br J Ophthalmol* 1984;68:182–7.
4 Brown SI. Mooren's ulcer treatment by conjunctival excision. *Br J Ophthalmol* 1975;59:670–82.
5 Cellin M, Fresina M, Strobbe E, *et al*. Corneoscleral graft in Mooren's ulcer: a case report (report online). *Cases J* 2009;180:e1–3. http://www.casesjournal.com/content/2/1/180 (accessed 7 Feb 2012).
6 Chow C, Foster CS. Mooren's ulcer. *Int Ophthalmol Clin* 1996;36:1–13.
7 Wakefield D, Robinson LP. Cyclosporin therapy in Mooren's ulcer. *Br J Ophthalmol* 1987;71:415–17.
8 Hill JC, Potter P. Treatment of Mooren's ulcer with cyclosporin A: report of three cases. *Br J Ophthalmol* 1987;71:11–15.
9 Tandon R, Chawla B, Verma K, *et al*. Outcome of treatment of Mooren ulcer with topical cyclosporine A 2%. *Cornea* 2008;27:859–61.
10 Kinoshita S, Ohashi Y, Ohji M, *et al*. Long-term results of keratoepithelioplasty in Mooren's ulcer. *Ophthalomology* 1991;98:438–45.
11 Brown SI, Mondino BJ, Rabin BS. Autoimmune phenomenon in Mooren's ulcer. *Am J Ophthalmol* 1976;82:835–40.
12 Gottsch JD, Liu SH, Minkovitz JB, *et al*. Autoimmunity to a cornea associated stromal antigen in patients with Mooren's ulcer. *Invest Ophthalmol Vis Sci* 1995;36:1541–7.
13 Young RD, Watson PG. Light and electron microscopy of corneal melting syndrome (Mooren's ulcer). *Br J Ophthalmol* 1982;66:341–56.
14 Yokoi N, Komuro A, Maruyama K, *et al*. New surgical treatment for superior limbic keratoconjunctivitis and its association with conjunctivochalasis. *Am J Ophthalmol* 2003;135:303–8.
15 Wang Z, Chen J, Zheng H. Changes in local immune functions in Mooren's ulcer. *Yan Ke Xue Bao* 1996;12:33–5.
16 Elliott JF, Lin Y, Mizel SB. Induction of interleukin 2 messenger RNA inhibited by cyclosporine A. *Science* 1984;226:1439–41.
17 Liu J, Farmer JD, Lane WS, *et al*. Calcineurin is a common target of cyclophilin–cyclosporin A and FKBP–FK506 complexes. *Cell* 1991;66:807–15.

Immunohistochemical analysis of inflammatory limbal conjunctiva adjacent to Mooren's ulcer

Katsuhiko Shinomiya, Mayumi Ueta, Chie Sotozono, et al.

Br J Ophthalmol 2013 97: 362-366 originally published online January 3, 2013
doi: 10.1136/bjophthalmol-2012-302631

Gene 516 (2013) 33–38

Contents lists available at SciVerse ScienceDirect

Gene

journal homepage: www.elsevier.com/locate/gene

Identification of a novel gene by whole human genome tiling array

Hirokazu Ishida [a,b], Tomohito Yagi [a], Masami Tanaka [a], Yuichi Tokuda [a], Kazumi Kamoi [b], Fumiya Hongo [b], Akihiro Kawauchi [b], Masakazu Nakano [a], Tsuneharu Miki [b], Kei Tashiro [a,*]

[a] Department of Genomic Medical Sciences, Graduate School of Medical Science, Kyoto Prefectural University of Medicine, Kyoto, Japan
[b] Department of Urology, Graduate School of Medical Science, Kyoto Prefectural University of Medicine, Kyoto, Japan

ARTICLE INFO

Article history:
Accepted 21 November 2012
Available online 19 December 2012

Keywords:
Tiling array
Microarray
Novel gene
Prostate

ABSTRACT

When the whole human genome sequence was determined by the Human Genome Project, the number of identified genes was fewer than expected. However, recent studies suggest that undiscovered transcripts still exist in the human genome. Furthermore, a new technology, the DNA microarray, which can simultaneously characterize huge amounts of genome sequence data, has become a useful tool for analyzing genetic changes in various diseases. A version of this tool, the tiling DNA microarray, was designed to search all the transcripts of the entire human genome, and provides huge amounts of data, including both exon and intron sequences, by a simple process. Although some previous studies using tiling DNA microarray analysis have indicated that numerous novel transcripts can be found in the human genome, none of them has reported any novel full-length human genes. Here, to find novel genes, we analyzed all the transcripts expressed in normal human prostate cells using this microarray. Because the optimal analytical parameters for using tiling DNA microarray data for this purpose had not been established, we established parameters for extracting the most likely regions for novel transcripts. The three parameters we optimized were the threshold for positive signal intensity, the Max gap, and the Min run, which we set to detect all transcriptional regions that were above the average length of known exons and had a signal intensity in the top 5%. We succeeded in obtaining the full-length sequence of one novel gene, located on chromosome 12q24.13. We named the novel gene "POTAGE". Its 5841-bp mRNA consists of 26 exons. We detected part of exon 2 in the tiling data analysis. The full-length sequence was then obtained by RT-PCR and RACE. Although the function of POTAGE is unclear, its sequence showed high homology with genes in other species, suggesting it might have an important or essential function. This study demonstrates that the tiling DNA microarray can be useful for identifying novel human genes.

1. Introduction

DNA microarray analysis has been established as one of the most useful technologies for investigating the underlying pathogenesis of various diseases (Castellano et al., 2009; Heintzman et al., 2009; Hussain et al., 2009; Takata et al., 2010; Xu et al., 2005; Yeager et al., 2007; Yeager et al., 2009). Annotated gene expression levels and single nucleotide polymorphisms can be conveniently evaluated using this technique. The tiling DNA microarray is a variation that was developed for investigating all the transcripts of the whole genome, including those of undiscovered genes (Bertone et al., 2004; Johnson et al., 2005; Kapranov et al., 2002; Mockler et al., 2005; Royce et al., 2005; Schadt et al., 2004; Shoemaker et al., 2001). This innovation also allows us to investigate the pathogenesis of various diseases.

The Human Genome Project reported the first complete sequence of the human genome in 2003. This project found 30,000 fewer expressed genes than had been expected (International Human Genome Sequencing Consortium, 2004; Lander et al., 2001; Venter et al., 2001). However, even though the findings also suggested that more than 98% of all genomic sequences are not transcribed (Cheng et al., 2005), recent studies on these "non-coding" DNA regions have revealed that they have many functions. In addition, these regions contain computationally predicted genes that may encode functional DNA and/or proteins. These observations suggest that novel genes that are transcribed into RNA may be found in these regions.

Because the original DNA microarray technology, used for evaluating annotated gene expression levels, was designed with relatively few probes, usually covering only the 5′-ends of annotated genes, it is not very useful for finding undiscovered transcripts in unexplored genomic regions. Specifically, the number and location of the probes meant that transcribed regions that lay between the probes could

Abbreviations: mRNA, messenger RNA; RT-PCR, reverse transcription-polymerase chain reaction; RACE, rapid amplification of cDNA ends; kb, kilobases; GAPDH, glyceraldehyde-3-phosphate dehydrogenase.

* Corresponding author at: Department of Genomic Medical Sciences, Kyoto Prefectural University of Medicine, Kawaramachi-Hirokoji, Kamigyo-ku, Kyoto, 602-8566, Japan. Tel.: +81 75 251 5346; fax: +81 75 251 5346.
E-mail address: tashiro@koto.kpu-m.ac.jp (K. Tashiro).

0378-1119/$ – see front matter © 2012 Elsevier B.V. All rights reserved.
http://dx.doi.org/10.1016/j.gene.2012.11.076

not be detected. In contrast, tiling DNA microarrays are useful for mapping novel transcripts, because the "tiling" feature consists of 25-mer oligonucleotide probes that are tiled at approximately 35-bp intervals, as measured from the central position of the adjacent probe. Therefore, a gap of only approximately 10 bp lies between probes, which cover the entire genome except the telomeres and centromeres (Sasaki et al., 2007). Tiling DNA microarray data have improved gene annotations and revealed the extensive transcriptions of non-coding RNAs. The closely spaced probes allow for the accurate measurement of small transcriptional features, such as single exons or small introns. This technology is now allowing us to investigate undiscovered transcripts as well as the expression of annotated genes. In this regard, the tiling DNA microarray is one of the most powerful and fruitful tools for evaluating both annotated genes and novel transcripts that have unclear functions. Previous reports using tiling DNA microarray have demonstrated novel transcripts in the human genome. However, full-length novel genes have not been reported (Kampa et al., 2004; Kapranov et al., 2005; Nelson et al., 2008; Weile et al., 2007).

In this study, we used tiling DNA microarray to seek undiscovered transcripts, and we demonstrated its usefulness for identifying a novel coding gene.

2. Materials and methods

2.1. Cell culture

Primary normal prostate epithelial cells (PrECs) were purchased from Lonza (Walkersville, MD) and maintained in prostate epithelial cell media (PrEGM Bullet Kit-Lonza) supplemented with a mixture of various growth factors (Single Quots-Lonza). Cells were seeded at recommended densities and cultured at 37 °C at 5% CO_2. Media were changed every 48 h.

2.2. RNA and DNA preparation

Total RNA was extracted from PrECs with the RNeasy Plus Mini Kit (Qiagen, Valencia, CA). RNA quality was evaluated by spectrophotometry with a NanoDrop ND-1000 spectrophotometer (Thermo Fisher Scientific, Wilmington, DE, USA) and by gel electrophoresis.

Genomic DNA was extracted from cancerous and normal frozen prostate tissue. The samples were minced and mixed well in lysis buffer with proteinase-K (to 0.2 mg/mL) and SDS (to 0.1%) at 55 °C. DNA was separated from the proteinaceous component by two extractions with an equal volume of phenol/chloroform isoamyl alcohol. The aqueous phase was mixed with 2.5 volumes of 100% ethanol and 0.1 volumes of 3 M sodium acetate and centrifuged at 12,000 ×*g* for 20 min at 4 °C. The DNA pellet was washed with cold 70% ethanol and allowed to air dry before resuspension in TE (10 mM Tris–HCl pH 7.5, 1 mM EDTA).

2.3. Affymetrix GeneChip® hybridization

Affymetrix Human Tiling 1.0R Array GeneChip® (Tiling array; Affymetrix, Santa Clara, CA) arrays were used for triplicate hybridizations. For the microarray hybridization, we followed the protocol described in the Affymetrix GeneChip® Whole Transcript Double-Stranded Target Assay Manual (Affymetrix, Santa Clara, CA). In brief, 6 μg of total RNA was purified by ribosomal RNA reduction using the RiboMinus Human/Mouse Transcriptome Isolation Kit (Invitrogen Co., Carlsbad, CA) and cleaned up. A single-stranded cDNA was synthesized using a T7-$(N)_6$ primer, and the cDNA was made double-stranded. The ds cDNA was amplified by in vitro transcription into complementary RNA (cRNA) and cleaned up. The second cycle ds cDNA was synthesized using the amplified cRNA as a template. The ds DNA was cleaned up, fragmented, and labeled with biotin. The fragmented ds DNA was used for hybridization to the microarrays at 45 °C for 16 h with a rotation rate of 60 rpm using a GeneChip® Hybridization Oven (Affymetrix, Santa Clara, CA). The microarrays were washed and stained using an Affymetrix GeneChip® Fluidics Station 450 and scanned by an Affymetrix GeneChip® Scanner 3000.

2.4. Tiling array data analysis

To handle the data generated by using probes that hybridize throughout the whole genome, we extracted the positive data as follows (Supplemental Fig. 1). As the distance used to locally group positional data for statistical analysis, we set the bandwidth at the maximum recommended level (73 bp). This setting increases the reliability of the signal intensity derived from a perfectly matched probe vs. a mismatched probe. After removing data that showed no signal intensity (43.9% of all probes in 14 arrays), the threshold for each array was set to filter out all but the top 5% of probe intensities. A positive probe was defined as one having a signal intensity greater than threshold (Supplemental Table 1, Supplemental Fig. 2) (Eisenberg and Levanon, 2003). To evaluate the DNA regions hybridizing with positive probes, we used a Max gap parameter (the maximum tolerated gap between positive positions in the derivation of detected regions) of 70 bp, to permit the hybridization of a negative probe between two positive probes. The Min run parameter (the minimum size of a detected region) was set at 140 bp, which is the approximate average length of all exons identified among the annotated genes of NCBI (http://www.ncbi.nlm.nih.gov/) Build 36.2 (Supplemental Table 1, Supplemental Fig. 3). The regions whose signals passed our three parameter settings were compared to those of annotated genes by the probe position, according to the information provided by NCBI Build 36 in the Affymetrix Integrated Genome Browser (IGB) (Nicol et al., 2009), to remove regions that overlapped with annotated genes. Next, the data were carefully divided into known or unknown transcripts by checking each sequence against the latest annotations. New transcripts that appeared within an annotated gene, even if not in the exonic sequences, were also considered to be gene-related transcripts, and we excluded them from further analysis. Finally, cases of two or more novel regions lying within 5-kbp on the genome were defined as "zones," and were investigated further.

2.5. RT-PCR and rapid amplification of cDNA ends (RACE)

Total RNA was extracted from the specimens using the RNeasy Plus Mini Kit (Qiagen, Valencia, CA). First-strand cDNA synthesis was performed using the SuperScript III First-Strand Synthesis System with an oligo $(dT)_{20}$ primer for RT-PCR (Invitrogen Co., Carlsbad CA), according to standard procedures.

Rapid amplification of cDNA ends (RACE) was performed with a GeneRacer kit (Invitrogen Co., Carlsbad, CA) and SMART RACE cDNA Amplification Kit (Clontech Laboratories, CA, USA), according to the manufacturer's instructions.

2.6. Sequencing analysis

Amplified RT-PCR and RACE products of target regions were sequenced with a BigDye terminator v1.1 or v3.1 Cycle Sequencing kit (Applied Biosystems, CA, USA) using Applied Biosystems 3130 Genetic Analyzers. The primers for the sequencing analysis were designed according to the results of each RACE analysis. The primer sequences are described in the supplementary information.

2.7. Quantitative RT-PCR assay in multiple human tissues

To evaluate the levels of POTAGE expression in human tissues, quantitative PCR (QPCR) was performed using the Stratagene Mx3005P

real-time QPCR system with the Brilliant II Fast SYBR Green QPCR Master Mix (Agilent Technologies, CA, USA) and Human MTC Panels I and II, which include heart, brain, placenta, lung, skeletal muscle, kidney, pancreas, spleen, thymus, prostate, testis, ovary, small intestine, colon, and peripheral leukocytes (Clontech Laboratories, CA, USA). These assays were performed at least four times in duplicate. To normalize the values in the quantitative assays, the level of *beta-Actin* was assessed as a control. The primer sequences for *beta-actin* were (forward) 5′-ATTGCCGACAGGATGCAGAA-3′ and (reverse) 5′-ACATC TGCTGGAAGGTGGACAG-3′. After the QRT-PCR assay, each sample was examined by agarose gel electrophoresis to evaluate the amplification of a single RT-PCR product.

2.8. Methylation assay with normal and cancerous human prostate tissue

DNA methylation is an important epigenetic mechanism of gene regulation. To investigate the methylation status of POTAGE in the human prostate, we performed methylation PCR using human prostate tissues. Normal and cancerous prostate samples were obtained from six patients, with their informed consent, during radical retropubic prostatectomy for clinically localized prostate adenocarcinoma, performed at the Kyoto Prefectural University of Medicine. All procedures were conducted in accordance with the Helsinki declaration. This study was approved by the Institutional Review Board of Kyoto Prefectural University of Medicine.

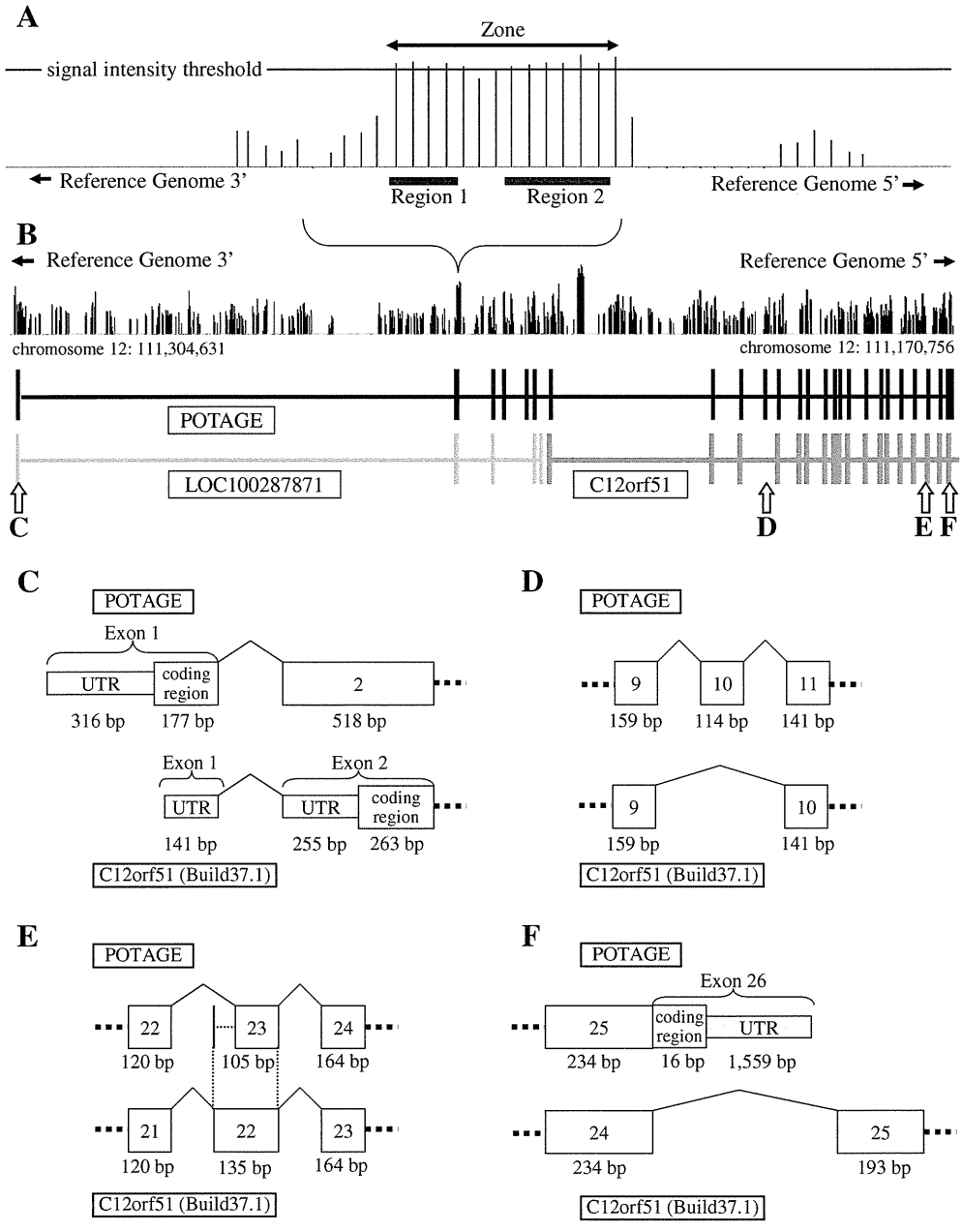

Fig. 1. (A) For this study, we defined two concepts: the region and the zone. A region was the genomic area that passed our settings for all three parameters and did not overlap with annotated genes. Zones were two or more regions that lay within 5-kbp of one another, on the chromosome. Zones were assumed to encode at least some portion of a novel gene. (B) Each novel zone was investigated in detail by RT-PCR and RACE. Shown is the region containing the novel protein, which overlapped with exon 2 of LOC100287871, a predicted gene in NCBI Build 36.3. We obtained the full-length mRNA sequence encoded by this region. (C, D, F) Although 22 of the 26 exons of the novel gene also served as exons of C12orf51, exons 1, 10, and 26 were new. (E) Exon 23 of the novel gene had a 30-bp deletion.

The genomic DNA samples from the six patients were treated with the MethylEasy Xceed Rapid DNA Bisulphite Modification Kit (Human Genetics Signatures Pty Ltd, Australia), according to the manufacturer's instructions. The methylation and unmethylation primers for POTAGE were designed using the CpG island searcher (http://cpgislands.usc.edu/) (Takai and Jones, 2003) and MethPrimer (http://www.urogene.org/methprimer/index1.html) web sites (Li and Dahiya, 2002). After the amplification, the PCR products were separated by electrophoresis on an agarose gel, and fragments in the expected range were excised and purified using the QIAquick Gel Extraction Kit (Qiagen, Valencia, CA). The purified PCR products were ligated using the pGEM-T Easy Vector System (Promega, WI, USA), and at least 20 independent clones were sequenced with the T7 (5′-TAATACGACTCACTATAGGG-3′) and SP6 (5′-ATTTAGGTGACACTATAGAA-3′) primers.

3. Results

3.1. Analysis of tiling array data

Our goal was to evaluate all the mRNAs expressed in human prostate cells, using the tiling array in triplicate. The signal intensity and P-value for each probe were determined by quantile normalization (Bolstad et al., 2003), after the raw intensity data from triplicate microarrays were transformed with the Affymetrix Tiling Analysis Software ver. 1.1. All of the extracted signal data were mapped to their genomic position and visualized in the IGB. Because the tiling array was designed based on information from NCBI Build 34, the results were translated to Build 36 automatically.

Because the thresholds determining positive signal intensity were determined on the basis of the signals from all the probes in each tiling array, the thresholds were slightly different for each array (see Materials and methods). The values for two other parameters (Max gap and Min run) were the same for all the arrays (see Materials and methods). The three parameter settings enabled us to predict the genomic locations likely to contain transcribed sequences. After comparing the sequences from our predicted regions with those of annotated genes (NCBI Build 37.1), we found 319 regions in the entire genomic sequence that encoded undiscovered transcripts. After the novel regions were obtained, the novel zones were defined by tiling data analysis. Finally, we defined 17 zones containing two or more regions within 5-kbp of each other (Fig. 1A, Supplemental Fig. 1 and Supplemental Table 1).

3.2. RT-PCR and RACE analysis of the novel region of human chromosome 12

We next designed primer sets for each region that were appropriate for performing RT-PCR analysis with the single-strand cDNA obtained from normal prostate cells. Each RT-PCR product was sequenced to confirm the amplification of the target sequences. Even when a positive tiling array signal was confirmed, no region was studied further without the successful amplification of the correct sequence. In addition, single regions that did not have any positive regions in the flanking regions were also excluded. After the RT-PCR analysis, primers for 5′- and 3′-RACE were designed on the basis of both the tiling array data and information from NCBI Build 37.1. All of the 5′- and 3′-RACE experiments were performed with single-stranded cDNA obtained from normal human prostate tissue.

Finally, we obtained the full-length sequence of POTAGE on chromosome 12q24.13 (Supplemental Table 2, primer Nos. 1–4, Supplemental Figs. 4, 5). However we succeeded to obtain the 17 zones by tiling array data, we failed to confirm 16 zones by RT-PCR and/or RACE.

The novel mRNA sequence we obtained consisted of 26 exons within an mRNA of 5841 bp. The gene was located on chromosome 12q24.13. Assuming that the tiling array data might indicate one of the exons in the novel transcripts, we performed RT-PCR and RACE of the regions in this zone. From these results, we found that 4 of the 6 5′-most exons of POTAGE belonged to the hypothetical protein LOC100287871 (http://www.ncbi.nlm.nih.gov/gene/?term=LOC100287871). Moreover, 18 of the 19 3′-most exons overlapped with part of the 5′-end of predicted gene C12orf51 in NCBI Build 37.1. There were three novel exons in POTAGE: exons 1, 10, and 26. Exon 23 of POTAGE contained a 30-bp deletion compared with the 5′-end of C12orf51 exon 22. The remaining 22 exons of POTAGE shared 100% identity with C12orf51 (Figs. 1B–F, Supplemental Table 3).

We also investigated the sequence flanking exons 25 and 26 of POTAGE in detail. We found at least two human isoforms of these exons. One isoform included exon 26 of POTAGE as its 3′-end; this isoform was equivalent to POTAGE. The other isoform had a different 3′-end; that is, some other exon followed exon 25. For example, C12orf51 was partially encoded by the other isoform.

To explore the possible function of POTAGE, motif and homology searches were performed using the MOTIF Search (http://motif.genome.jp/), Pfam (http://pfam.sanger.ac.uk/), and NCBI web sites. No major motif was found in the nucleotide acid sequence or the deduced protein sequence.

3.3. Comparison of POTAGE expression level in multiple human tissues

We evaluated the expression levels of POTAGE with region-specific primer pairs in multiple human tissues (Human MTC Panels I and II), using semi-quantitative real-time RT-PCR (Supplemental Table 2, primer No. 5). POTAGE was expressed in every human tissue examined. The relative expression levels were calculated as the levels normalized to the beta-actin expression in each sample. The highest expression level of POTAGE was observed in the testis (Fig. 2). We created primer pairs to evaluate the level of expression of the other isoform, and performed real time RT-PCR using the same conditions as for POTAGE. While the expression level of the other isoform also was higher in testis, it was different from that of POTAGE, in that the other isoform was also highly expressed in skeletal muscle (data not shown).

3.4. Methylation assay for the 5′-upstream CG-rich region of POTAGE

Because DNA methylation in the 5′-upstream CG-rich region of a gene is related to the repression of gene expression, we investigated the methylation status of POTAGE using a methylation-specific PCR assay, to discover if differences in methylation could explain the lower expression level of POTAGE in normal prostate tissue compared to other tissues (Jones and Baylin, 2007; Laird, 2003; Ting et al., 2006;

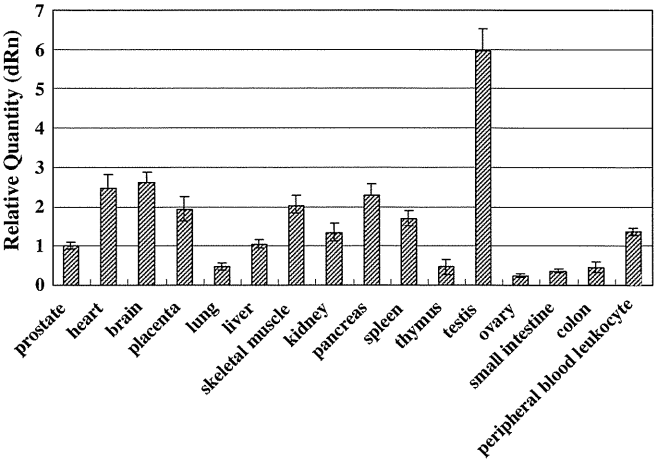

Fig. 2. The expression levels of the novel gene in multiple human tissues using semi-quantitative real-time RT-PCR. The novel gene was expressed in every human tissue examined in this study, and its level was highest in the testis.

Table 1
Homology among exons of the novel gene in human, mouse, rat, and fugu (pufferfish).

		cDNA (translated region)			
		Human	Mouse	Rat	Fugu
Amino acids	Human		89.18%	88.80%	70.60%
	Mouse	97.27%		95.14%	72.59%
	Rat	97.05%	98.19%		72.47%
	Fugu	81.15%	81.00%	80.92%	

The percentage of identical amino acids was essentially constant across species.

Vanaja et al., 2009). In addition, we examined the methylation condition in prostate cancer tissue, to assess any relationship between the level of expression and prostate oncogenesis. We examined the methylation of CpG 101 (UCSC (http://genome.ucsc.edu/) GRCh37/hg39), a CpG island located 557 bp upstream of POTAGE (Supplemental Table 2, Nos. 6–7, Supplemental Fig. 6). However, the CpG island was not methylated in normal or cancerous prostate tissues.

4. Discussion

New genomic technologies have yielded much useful information about the whole human genome, and both experimental and computational approaches have been developed to handle the accumulation of data. Our approach using the tiling array supported the importance of choosing the appropriate settings for the three parameters, threshold of signal intensity, Max gap, and Min run, when examining the tiling data to evaluate mRNA expression or discover novel genes. The settings of these parameters were critical to our finding the few pieces of relevant information among the enormous quantities of tiling array data. Because our data demonstrated that the signal patterns of many undiscovered regions were very short or very close to annotated genes, we excluded unknown regions with these patterns to obtain novel genes that were independent of the known genes. Therefore, the three parameters in our data were chosen to be stringent, to reduce the amount of data that would require further investigation.

First, our parameter settings allowed us to extract 17 zones containing novel regions from our entire set of tiling array data. All of the zones consisted of two or more novel regions within about 5-kbp of one another. We assumed that each novel region might represent one or more exons of a novel gene. In 16 of the 17 zones, each region was confirmed as encoding a transcript. However, no amplification product included neighboring sequences.

Finally, we determined the sequence of a full-length novel gene from the RT-PCR and RACE results of 1 of the 17 zones. The novel mRNA was 5841 bp in length and contained 26 exons, which were encoded by sequences spread over 133,876 bp in the genome, on chromosome 12q24.13. There were two predicted genes, hypothetical protein LOC100287871 and C12orf51, that were close to our discovered gene (NCBI Build 36.3). The information on hypothetical protein LOC100287871 was replaced with the predicted region of C12orf51 in NCBI Build 37.1. To confirm the sequence of POTAGE, we also referred to the sequence of the predicted transcript at NCBI Build 37.1.

Among the 26 exons of POTAGE, three were novel (exons 1, 10, and 26). POTAGE also shared 23 exons with C12orf51 (NCBI Build 37.1), and the 22nd exon of POTAGE (the 23rd exon of C12orf51) contained a 30-bp deletion.

The expression level of POTAGE was lower in the prostate than in most other tissues. To investigate whether POTAGE's expression was suppressed by methylation, we examined the genomic methylation in the 5′-upstream CpG island of POTAGE in normal prostate and prostate cancer, to look for possible associations between malignancies and expression of POTAGE. However, the region we assayed was not methylated in normal or cancerous prostate tissue. Therefore, the different expression levels in several tissues, including prostate cancer, are unlikely to be regulated by the methylation of the 5′-upstream CG rich region of POTAGE.

POTAGE has no major motif in the nucleotide acid sequence or the deduced protein sequence. Interestingly, the sequence of POTAGE had high homology to transcripts in other species, such as mouse and rat. The predicted protein had a 97% sequence identity between human and mouse, and almost the same homology between human and rat (Table 1). The alignment of the amino acid sequences, which was constructed using CLUSTAL W ver. 1.83 (http://clustalw.ddbj.nig.ac.jp/top-j.html) with Kimura's correction, between human and five other species, showed the closest matches among different species (Supplemental Fig. 7). Furthermore, the phylogenetic relationship based on the amino acid alignments of these six species also revealed high protein homology among human and other species (Fig. 3). On the other hand, the nucleotide sequence identities between human and mouse of two housekeeping proteins (beta-Actin and GAPDH) are 92% and 89%. The between-species percent identity of POTAGE was higher than that of these housekeeping genes. Therefore, although the function of POTAGE is currently unknown, its high sequence homology among different species suggests that it may have an important or essential biological function.

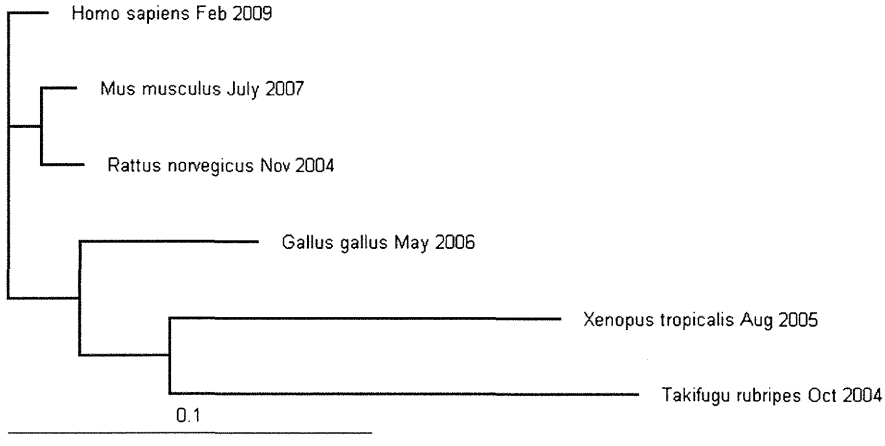

Fig. 3. Phylogram depicting the relationship between the deduced amino acid sequence encoded by the novel gene in humans and its homologues in five other species, using Tree View (ver. 1.6.6). The phylogram was based on the alignment of the amino acid sequences (see Supplemental Fig. 7).

In summary, we identified a novel gene in a search of the whole human genome using the powerful new tiling array tool. Although analyzing the tiling array data was no simple matter, it was still useful for detecting a novel gene.

Supplementary data to this article can be found online at http://dx.doi.org/10.1016/j.gene.2012.11.076.

Acknowledgments

T. Ichikawa is thanked for excellent secretarial assistance. R. Sato and F. Sato (SASA Plus Co., Ltd., Fukuoka, Japan) are thanked for the assistant of data management and the development of the specific tool for sequence analysis. This work was supported by grants from Grants-in-Aid for Scientific Research.

References

Bertone, P., et al., 2004. Global identification of human transcribed sequences with genome tiling arrays. Science 306, 2242–2246.
Bolstad, B.M., Irizarry, R.A., Astrand, M., Speed, T.P., 2003. A comparison of normalization methods for high density oligonucleotide array data based on variance and bias. Bioinformatics 19, 185–193.
Castellano, L., et al., 2009. The estrogen receptor-alpha-induced microRNA signature regulates itself and its transcriptional response. Proc. Natl. Acad. Sci. U. S. A. 106, 15732–15737.
Cheng, J., et al., 2005. Transcriptional maps of 10 human chromosomes at 5-nucleotide resolution. Science 308, 1149–1154.
Eisenberg, E., Levanon, E.Y., 2003. Human housekeeping genes are compact. Trends Genet. 19, 362–365.
Heintzman, N.D., et al., 2009. Histone modifications at human enhancers reflect global cell-type-specific gene expression. Nature 459, 108–112.
Hussain, M., et al., 2009. Tobacco smoke induces polycomb-mediated repression of Dickkopf-1 in lung cancer cells. Cancer Res. 69, 3570–3578.
International Human Genome Sequencing Consortium, 2004. Finishing the euchromatic sequence of the human genome. Nature 431, 931–945.
Johnson, J.M., Edwards, S., Shoemaker, D., Schadt, E.E., 2005. Dark matter in the genome: evidence of widespread transcription detected by microarray tiling experiments. Trends Genet. 21, 93–102.
Jones, P.A., Baylin, S.B., 2007. The epigenomics of cancer. Cell 128, 683–692.
Kampa, D., et al., 2004. Novel RNAs identified from an in-depth analysis of the transcriptome of human chromosomes 21 and 22. Genome Res. 14, 331–342.
Kapranov, P., et al., 2002. Large-scale transcriptional activity in chromosomes 21 and 22. Science 296, 916–919.
Kapranov, P., et al., 2005. Examples of the complex architecture of the human transcriptome revealed by RACE and high-density tiling arrays. Genome Res. 15, 987–997.
Laird, P.W., 2003. The power and the promise of DNA methylation markers. Nat. Rev. Cancer 3, 253–266.
Lander, E.S., et al., 2001. Initial sequencing and analysis of the human genome. Nature 409, 860–921.
Li, L.C., Dahiya, R., 2002. MethPrimer: designing primers for methylation PCRs. Bioinformatics 18, 1427–1431.
Mockler, T.C., Chan, S., Sundaresan, A., Chen, H., Jacobsen, S.E., Ecker, J.R., 2005. Applications of DNA tiling arrays for whole-genome analysis. Genomics 85, 1–15.
Nelson, C.M., et al., 2008. Whole genome transcription profiling of *Anaplasma phagocytophilum* in human and tick host cells by tiling array analysis. BMC Genomics 9, 364.
Nicol, J.W., Helt, G.A., Blanchard Jr., S.G., Raja, A., Loraine, A.E., 2009. The Integrated Genome Browser: free software for distribution and exploration of genome-scale datasets. Bioinformatics 25, 2730–2731.
Royce, T.E., et al., 2005. Issues in the analysis of oligonucleotide tiling microarrays for transcript mapping. Trends Genet. 21, 466–475.
Sasaki, D., Kondo, S., Maeda, N., Gingeras, T.R., Hasegawa, Y., Hayashizaki, Y., 2007. Characteristics of oligonucleotide tiling arrays measured by hybridizing full-length cDNA clones: causes of signal variation and false positive signals. Genomics 89, 541–551.
Schadt, E.E., et al., 2004. A comprehensive transcript index of the human genome generated using microarrays and computational approaches. Genome Biol. 5, R73.
Shoemaker, D.D., et al., 2001. Experimental annotation of the human genome using microarray technology. Nature 409, 922–927.
Takai, D., Jones, P.A., 2003. The CpG island searcher: a new WWW resource. Silico Biol, 3, pp. 235–240.
Takata, R., Akamatsu, S., Kubo, M., Takahashi, A., Hosono, N., Kawaguchi, T., Tsunoda, T., Inazawa, J., Kamatani, N., Ogawa, O., Fujioka, T., Nakamura, Y., Nakagawa, H., 2010. Genome-wide association study identifies five new susceptibility loci for prostate cancer in the Japanese population. Nat. Genet. 42, 751–754.
Ting, A.H., McGarvey, K.M., Baylin, S.B., 2006. The cancer epigenome—components and functional correlates. Genes Dev. 20, 3215–3231.
Vanaja, D.K., et al., 2009. Hypermethylation of genes for diagnosis and risk stratification of prostate cancer. Cancer Invest. 27, 549–560.
Venter, J.C., et al., 2001. The sequence of the human genome. Science 291, 1304–1351.
Weile, C., Gardner, P.P., Hedegaard, M.M., Vinther, J., 2007. Use of tiling array data and RNA secondary structure predictions to identify noncoding RNA genes. BMC Genomics 8, 244.
Xu, J., et al., 2005. A combined genomewide linkage scan of 1,233 families for prostate cancer-susceptibility genes conducted by the international consortium for prostate cancer genetics. Am. J. Hum. Genet. 77, 219–229.
Yeager, M., et al., 2007. Genome-wide association study of prostate cancer identifies a second risk locus at 8q24. Nat. Genet. 39, 645–649.
Yeager, M., et al., 2009. Identification of a new prostate cancer susceptibility locus on chromosome 8q24. Nat. Genet. 41, 1055–1057.

Remarks on Equivariant and Isovariant Maps between Representations

Ikumitsu NAGASAKI

STUDIA HUMANA et NATURALIA

No.47

京都府立医科大学医学部医学科

Kyoto Prefectural University of Medicine

2013年12月抜刷

Remarks on Equivariant and Isovariant Maps between Representations

Ikumitsu NAGASAKI [1)]

Abstract. In this note, we consider the existence problem of equivariant or isovariant maps between representation spheres. In particular, we give a necessary and sufficient condition for the existence of an equivariant map between unitary representation spheres of a cyclic group C_{pq}, where p, q are distinct primes.

1. The existence problem of C_{pq}-maps

The existence or non-existence problem of equivariant maps is a fundamental and important topic in equivariant topology, and many results are known up to the present. However, giving a necessary and sufficient condition for the existence of an equivariant map is not so easy in general. Recently, Marzantowicz, de Mattos and dos Santos [6] discuss a necessary and sufficient condition of the existence of an equivariant map for a torus and a p-torus. In this note, we deal with the case of C_{pq}-maps, where p, q are distinct primes.

First, we recall well-known results on the existence problem. Let G be a compact Lie group and V an (orthogonal) representation of G. We denote by SV the representation sphere of V, which is defined as the unit sphere of V. The following fact is proved by equivariant obstruction theory; for example, see [2].

Proposition 1.1. *Let V and W be (orthogonal) representations of G. If $\dim V^H \leq \dim W^H$ for every (closed) subgroup H of G, then there exists a G-map $f\colon SV \to SW$.*

The converse is not true in general, but in some special cases, the converse holds. Such kind of results are brought from Borsuk-Ulam type theorems. We state two Borsuk-Ulam type theorems; see [3], [4], [5], [11] for more details.

[1)] Department of Mathematics, Kyoto Prefectural University of Medicine, 13 Nishitakatsukasa-cho, Taishogun, Kita-ku, Kyoto 603-8334, Japan. e-mail: nagasaki@koto.kpu-m.ac.jp

2010 *Mathematics Subject Classification.* Primary 57S17; Secondary 55M20.

Proposition 1.2. *Assume that G acts freely on SV and SW. If there exists a G-map $f\colon SV \to SW$, then $\dim V \leq \dim W$ holds.*

Proposition 1.3. *Let G be a torus T^n or a p-torus C_p^n. Assume that SV and SW are G-fixed point free, i.e., $SV^G = SW^G = \emptyset$. If there exists a G-map $f\colon SV \to SW$, then $\dim V \leq \dim W$ holds.*

Marzantowicz, de Mattos and dos Santos [6] give a necessary and sufficient condition for the existence of an equivariant map in the case of G being a torus or a p-torus. In particular, the following result is deduced from their results.

Corollary 1.4. *Let G be a torus T^n or a p-torus C_p^n. Let SV and SW be G-fixed point free representation spheres. Then there exists a G-map $f\colon SV \to SW$ if and only if $\dim V^H \leq \dim W^H$ holds for every closed subgroups H of G.*

Proof. Note that G/H is a torus or a p-torus; in fact, if $G = T^n$, then G/H is connected and abelian. Hence G/H is a torus. If $G = C_p^n$, then G/H is an abelian group consisting of elements of order p or 1. Hence G/H is a p-torus. In each case, $f^H\colon SV^H \to SW^H$ is a G/H-map between G/H-fixed point free representation spheres. Hence Proposition 1.3 shows the necessary condition. The sufficient condition follows from Proposition 1.1. □

We now consider equivariant maps between representation spheres of a cyclic group C_{pq}, where p, q are distinct primes. Let $G = C_{pq}$ and c a generator of C_{pq}. The unitary irreducible representations U_k $(0 \leq k \leq pq-1)$ of C_{pq} are given by

$$cz = \xi^k z \quad \text{for} \quad z \in U_k = \mathbb{C},\ \xi = \exp\frac{2\pi\sqrt{-1}}{pq}.$$

Each orthogonal irreducible representation T_k is given as the following way: $T_0 = \mathbb{R}$ with the trivial action; if $0 < k < pq/2$, then $T_k = r_{\mathbb{R}}U_k$, where $r_{\mathbb{R}}$ denote realification of a unitary representation, and if $q = 2$ and p is an odd prime, then $T_p = \mathbb{R}_-$ with the antipodal action of C_2 and the trivial action of C_p.

Set $C_p = \langle c^q \rangle$ and $C_q = \langle c^p \rangle$. Let V and W be orthogonal representations with $V^G = W^G = 0$. If there exists a G-map $f\colon SV \to SW$, then $f^H\colon SV^H \to SW^H$ is a G/H-map for $H = C_p$ or C_q. Since G/H acts freely on SV^H and SW^H, it follows from Proposition 1.2 that $\dim V^H \leq \dim W^H$ for $H = C_p$, C_q. In the case of $\dim W^H = 0$ $(H = C_p$ or $C_q)$, it follows that $\dim V^H = 0$. Since $\mathrm{res}_H f$ is an H-map between H-free

representation spheres, we have $\dim V \leq \dim W$ by Proposition 1.2. Thus we obtain the following.

Proposition 1.5. *Let $G = C_{pq}$. Let V and W be representations with $V^G = W^G = 0$. If there exists a G-map $f: SV \to SW$, then the following hold.*

(1) $\dim V^{C_p} \leq \dim W^{C_p}$ *and* $\dim V^{C_q} \leq \dim W^{C_q}$.

(2) *If* $\dim W^{C_p} = 0$ *or* $\dim W^{C_q} = 0$, *then* $\dim V \leq \dim W$.

In the next section, we show that if V and W are unitary, then the converse holds. As a consequence, we obtain the following.

Theorem 1.6. *Let V and W be unitary representations with $V^G = W^G = 0$ for $G = C_{pq}$. There exists a G-map $f: SV \to SW$ if and only if the conditions* (1) *and* (2) *of Proposition* 1.5 *hold.*

2. Proof of Theorem 1.6

We have already shown that the conditions (1) and (2) are necessary. Next we show that (1) and (2) are sufficient for the existence of a G-map. The proof is divided into several cases.

We set $G = C_{pq}$ and denote by U_k the unitary irreducible representation of C_{pq} described in the previous section. The following is straightforward.

Lemma 2.1. *If $f_i: SV_i \to SW_i$, $i = 1, 2$, are G-maps, then the join of f_1 and f_2 induces a G-map $f_1 * f_2: S(V_1 \oplus V_2) \to S(W_1 \oplus W_2)$.*

The kernel $\operatorname{Ker} V$ of a representation V is defined by the kernel of the representation homomorphism of V: $\rho_V: G \to GL(V)$. It is easily seen that

$$\operatorname{Ker} U_k = \begin{cases} 1 & (k, pq) = 1 \\ C_p & (k, pq) = p \\ C_q & (k, pq) = q \\ C_{pq} & k = 0, \end{cases}$$

where (k, pq) denotes the greatest common divisor of k and pq.

Lemma 2.2. *If $\operatorname{Ker} U_k = \operatorname{Ker} U_l$, then there exists a G-map $f: SU_k \to SU_l$.*

Proof. If $\operatorname{Ker} U_k = \operatorname{Ker} U_l = C_{pq}$, then it is trivial. Assume that $\operatorname{Ker} U_k = \operatorname{Ker} U_l \neq C_{pq}$ Since $(k/(k, pq), pq) = 1$, one can take an integer s such that $sk/(k, pq) \equiv 1 \pmod{pq}$.

Then a map f defined by

$$f(z) = z^{sl/(k,pq)},\ z \in SU_k$$

is a G-map. □

For a representation V with $V^G = 0$, decompose V into irreducible representations as follows:

$$V = \bigoplus_{i=1}^{pq-1} a_i U_i\ (a_i \geq 0).$$

Let H be a subgroup of G. Setting $V(H) = \bigoplus_{i:\mathrm{Ker}\, U_i = H} a_i U_i$, we have a decomposition

$$V = V(1) \oplus V(C_p) \oplus V(C_q).$$

By Lemmas 2.1 and 2.2, we obtain the following.

Proposition 2.3. *There exist G-maps between $S(V(H))$ and $S(mU_{(|H|,pq)})$ bidirectionally, where $m = \frac{1}{2}\dim V(H)$.*

By this proposition, without loss of generality, we may assume that V and W have the following forms:

$$V = a_1 U_1 \oplus a_p U_p \oplus a_q U_q,$$
$$W = b_1 U_1 \oplus b_p U_p \oplus b_q U_q,$$

where a_i and b_i are non-negative integers. Note that $V^{C_p} = a_p U_p$, $V^{C_q} = a_q U_q$ and so on. It is easy to see that the conditions (1) and (2) are equivalent to statements:

(1) $a_p \leq b_p$ and $a_q \leq b_q$.

(2) If $b_p = 0$, then $a_1 + a_q \leq b_1 + b_q$ and if $b_q = 0$, then $a_1 + a_p \leq b_1 + b_p$.

First we recall the following result from [12].

Lemma 2.4. *Let $W = b_1 U_1 \oplus b_p U_p \oplus b_q U_q$, $b_p > 0$, $b_q > 0$. Then there exists a self G-map $h\colon SW \to SW$ such that $\deg h = 0$.*

Proof. Degrees of h^H, $H \leq G$, of a self G-map h on SW satisfy the Burnside ring relation described in [2]. In fact, it is seen that if there exists a G-map $h\colon SW \to SW$, then the following relations hold:

$$\begin{cases} \deg h \equiv \deg h^{C_p} \bmod p, \\ \deg h \equiv \deg h^{C_q} \bmod q, \\ \deg h^{C_p} \equiv 1 \bmod q, \\ \deg h^{C_q} \equiv 1 \bmod p. \end{cases}$$

Conversely, if integers d_1, d_p, d_q satisfy relations $d_1 \equiv d_p \bmod p$, $d_1 \equiv d_q \bmod q$, $d_p \equiv 1 \bmod q$ and $d_q \equiv 1 \bmod p$, then there exists a G-map $h\colon SW \to SW$ such that $\deg h = d_1$, $\deg h^{C_p} = d_p$, $\deg h^{C_q} = d_q$. We set $d_1 = 0$ and we can take d_p such that $d_p \equiv 0 \bmod p$, $d_p \equiv 1 \bmod q$ and d_q such that $d_q \equiv 1 \bmod p$, $d_q \equiv 0 \bmod q$, These integers satisfy the above relations. Therefore there exists a G-map $h\colon SW \to SW$ such that $\deg h = 0$. □

2.1. **Case 1.** We shall show the theorem when $b_p > 0$ and $b_q > 0$.

Lemma 2.5. *If* (1) $a_p \leq b_p$, $a_q \leq b_q$ *and* (2) $b_p > 0$, $b_q > 0$, *then there exists a* G*-map* $f\colon SV \to SW$.

Proof. By (1), there is an inclusion $i\colon SV^{>1} \to SW^{>1} \subset SW$. Using Waner's method [12], we show that this inclusion can be extended to a G-map f. Since G acts freely on $SV \setminus SV^{>1}$, SV is decomposed as a union of $SV^{>1}$ and free G-cells:

$$SV = SV^{>1} \cup G \times D^{n_1} \cup \cdots \cup G \times D^{n_r},$$

where $n_1 \leq \cdots \leq n_r$. Set $X_k = SV^{>1} \cup G \times D^{n_1} \cup \cdots \cup G \times D^{n_k}$, where $k \geq 1$. Suppose inductively that there is a G-map $f_{k-1}\colon X_{k-1} \to SW$, where $X_0 = SV^{>1}$ and $f_0 = i$. Since $X_k = X_{k-1} \cup G \times D^{n_k}$, restricting f_{k-1} to $1 \times \partial D^{n_k} = \partial D^{n_k}$, we have a map $g = f_{k-1}|_{\partial D^{n_k}}\colon \partial D^{n_k} \to SW$. Compose g with a G-map h of degree 0 and set $g' = h \circ g$. Then g' is null-homotopic and g' is extended to $g''\colon D^{n_k} \to SW$. Furthermore, g'' is equivariantly extended to a G-map $\tilde{g}\colon G \times D^{n_k} \to SW$. Thus we obtain a G-map $f_k = f_{k-1} \cup \tilde{g}\colon X_k \to SW$. □

2.2. **Case 2.** We shall show the theorem in the case of $b_p = 0$ or $b_q = 0$. We may suppose $b_q = 0$. Then by condition (1), we have $a_q = 0$ and $a_p \leq b_p$, If $a_1 \leq b_1$, then, there is an inclusion $i\colon SV \to SW$, which is G-equivariant.

Suppose that $a_1 > b_1$. By condition (2), we have $a_1 + a_p \leq b_1 + b_p$ and hence $a_1 - b_1 \leq b_p - a_p$. Note that there exists a G-map $g\colon SU_1 \to SU_p$; for example, g can be defined by $g(z) = z^p$. Hence there exists a G-map $\bar{g}\colon S((a_1-b_1)U_1) \to S((b_p-a_p)U_p)$ by Lemma 2.1. Joining $\bar{g}$ with the identity map $id\colon S(b_1U_1 \oplus a_pU_p) \to S(b_1U_1 \oplus a_pU_p)$, we obtain a G-map $f = \bar{g} * id\colon SV \to SW$. Thus the proof is complete.

3. Comparison to isovariant maps

Let G be a compact Lie group. A continuous G-map $f\colon X \to Y$ is called G-isovariant if f preserves the isotropy groups; i.e., $G_{f(x)} = G_x$ for all $x \in X$. It is

important to clarify the existence problem of isovariant maps and there are several researches about isovariant map as well as equivariant maps; for example, see [7], [8], [9], [10]. A necessary and sufficient condition for the existence of a C_{pq}-isovariant map between representations (or equivalently, representation spheres) is already known. In fact, the following result easily follows from results of [7].

Proposition 3.1. *Let $G = C_{pq}$. Let SV and SW be G-fixed point free (orthogonal) representation spheres. There exits a G-isovariant map $f\colon SV \to SW$ if and only if*

(1) $\dim V^H \leq \dim W^H$ *for* $H = C_p$ *and* C_q, *and*

(2) $\dim V - \dim V^H \leq \dim W - \dim W^H$ *for* $H = C_p$ *and* C_q.

Remark. By combining (1) and (2), it is deduced that $\dim V \leq \dim W$. This kind of result is called the isovariant Borsuk-Ulam theorem. See [10], [13] for more general results.

By comparing Proposition 3.1 and Theorem 1.6, we see that there are many pairs SV, SW of C_{pq}-fixed point free representation spheres such that there is a C_{pq}-map from SV to SW, but not a C_{pq}-isovariant map.

Example 3.2. Let $V = aU_1$ $(a \geq 1)$ and $W = U_p \oplus U_q$. Then there is a C_{pq}-map $f\colon SV \to SW$. However, if $a \geq 2$, then there is no C_{pq}-isovariant map from SV to SW.

This example provides another kind of Borsuk-Ulam type result; namely, if $a \geq 2$ and $f\colon SV \to SW$ is a C_{pq}-map, then it follows that $f^{-1}(SW^{>1}) \neq \emptyset$, where $SW^{>1}$ denotes the singular set of SW defined by $SW^{>1} = \{x \in SW \mid G_x \neq 1\}$. In this case, note that $SW^{>1} = SU_p \coprod SU_q$ (Hopf link). Furthermore, one can show the following.

Proposition 3.3. *Let $V = aU_1$ $(a \geq 2)$ and $W = U_p \oplus U_q$. If there is a C_{pq}-map $f : SV \to SW$, then $f^{-1}(SU_p) \neq \emptyset$ and $f^{-1}(SU_q) \neq \emptyset$.*

Proof. If $f^{-1}(SU_p) = \emptyset$, then we have an equivariant map $f\colon SV \to SW \setminus SU_p$. Since $SW \setminus SU_p$ is C_{pq}-homotopy equivalent to SU_q, there exists a C_{pq}-map $g\colon SV \to SU_q$. However, this contradicts Proposition 1.5 (2). Thus we see that $f^{-1}(SU_p) \neq \emptyset$. Similarly we see that $f^{-1}(SU_q) \neq \emptyset$. □

References

[1] T. Bartsch, *On the existence of Borsuk-Ulam theorems*, Topology **31** (1992), 533–543.

[2] T. tom Dieck, Transformation groups, *Transformation Groups*, Walter de Gruyter, Berlin, New York, 1987.

[3] E. Fadell and S. Husseini, *An ideal-valued cohomological index theory with applications to Borsuk-Ulam and Bourgin–Yang theorems*, Ergodic Theory Dynamical System **8** (1988), 73–85.

[4] T. Kobayashi, *The Borsuk-Ulam theorem for a $\mathbb{Z}_q$-map from a $\mathbb{Z}_q$-space to S^{2n+1}*, Proc. Amer. Math. Soc. 97 (1986), 714–716.

[5] W. Marzantowicz, *Borsuk-Ulam theorem for any compact Lie group*, J. Lond. Math. Soc., II. Ser. 49 (1994),195–208.

[6] W. Marzantowicz, D. de Mattos and E. L. dos Santos, *Bourgin-Yang version of the Borsuk-Ulam theorem for p-toral groups*, preprint.

[7] I. Nagasaki, *The converse of isovariant Borsuk-Ulam results for some abelian groups*, Osaka. J. Math. **43** (2006), 689-710.

[8] I. Nagasaki, *A note on the existence problem of isovariant maps between representation spaces*, Studia Humana et Naturalia 43 (2009), 33–42.

[9] I. Nagasaki, *Remarks on Borsuk-Ulam type results and the existence of isovariant maps*, Studia Humana et Naturalia 44 (2010), 91–100.

[10] I Nagasaki and F. Ushitaki, *New examples of the Borsuk-Ulam groups*, RIMS Kôkyuûoku Bessatsu **B39** (2013), 109–119.

[11] I. Nagasaki, T. Kawakami, Y. Hara and F. Ushitaki, *The Smith homology and Borsuk-Ulam type theorems*, Far East Journal of Mathematical Sciences (FJMS) **38** (2) (2010), 205-216.

[12] S. Waner, *A note on the existence of G-maps between spheres*, Proc. Amer. Math. Soc. **99** (1987), 179-181.

[13] A. G. Wasserman, *Isovariant maps and the Borsuk-Ulam theorem*, Topology Appli. **38** (1991), 155–161.

Bai et al. Molecular Brain 2013, 6:34
http://www.molecularbrain.com/content/6/1/34

Molecular Brain

RESEARCH Open Access

NMDA receptor subunits have different roles in NMDA-induced neurotoxicity in the retina

Ning Bai[1,4*], Tomomi Aida[1], Michiko Yanagisawa[1], Sayaka Katou[1], Kenji Sakimura[5], Masayoshi Mishina[6] and Kohichi Tanaka[1,2,3*]

Abstract

Background: Loss of retinal ganglion cells (RGCs) is a hallmark of various retinal diseases including glaucoma, retinal ischemia, and diabetic retinopathy. N-methyl-D-aspartate (NMDA)-type glutamate receptor (NMDAR)-mediated excitotoxicity is thought to be an important contributor to RGC death in these diseases. Native NMDARs are heterotetramers that consist of GluN1 and GluN2 subunits, and GluN2 subunits (GluN2A–D) are major determinants of the pharmacological and biophysical properties of NMDARs. All NMDAR subunits are expressed in RGCs in the retina. However, the relative contribution of the different GluN2 subunits to RGC death by excitotoxicity remains unclear.

Results: GluN2B- and GluN2D-deficiency protected RGCs from NMDA-induced excitotoxic retinal cell death. Pharmacological inhibition of the GluN2B subunit attenuated RGC loss in glutamate aspartate transporter deficient mice.

Conclusions: Our data suggest that GluN2B- and GluN2D-containing NMDARs play a critical role in NMDA-induced excitotoxic retinal cell death and RGC degeneration in glutamate aspartate transporter deficient mice. Inhibition of GluN2B and GluN2D activity is a potential therapeutic strategy for the treatment of several retinal diseases.

Keywords: NMDA receptor, GluN2B, GluN2D, Excitotoxicity, Retina, Glaucoma, Glutamate transporter

Background

Glutamate is the major excitatory neurotransmitter in the mammalian central nervous system. However, its accumulation in extracellular spaces kills neurons through excitotoxic mechanisms via activation of glutamate receptors [1]. Excitotoxic neuronal cell death is thought to be a final common pathway in various neurological diseases, ranging from acute ischemic stroke to chronic neurodegenerative diseases such as Alzheimer's disease and amyotrophic lateral sclerosis [2-5]. Glutamate excitotoxicity has also been proposed to be an important contributor to the death of retinal ganglion cells (RGCs) in glaucoma and ischemia-related conditions such as vessel occlusion and diabetic retinopathy [6-8], although some investigations have failed to confirm elevated glutamate concentration both in human patients with glaucoma [9] and in animal models of glaucoma [10,11]. The toxic effects of glutamate on RGCs are predominantly mediated by the overstimulation of N-methyl-D-aspartate (NMDA)-type glutamate receptors (NMDARs) due to their extreme permeability to calcium ions [12].

NMDARs are composed of various combinations of GluN1 and GluN2 (GluN2A–GluN2D) subunits and, in some cases, GluN3 (GluN3A and GluN3B) subunits. GluN2 subunits are major determinants of the functional properties of NMDARs, including characteristics such as agonist affinity, deactivation kinetics, single-channel conductance, Ca^{2+} permeability, and sensitivity to Mg^{2+} [13]. However, the relative contribution of different GluN2 subunits to RGC death by excitotoxicity remains unclear.

We previously reported that NMDAR-mediated excitotoxicity contributed to the degeneration of RGCs in glutamate aspartate transporter (GLAST) deficient (KO)

* Correspondence: bai.ning.aud@mri.tmd.ac.jp; tanaka.aud@mri.tmd.ac.jp
[1]Laboratory of Molecular Neuroscience, Medical Research Institute, Tokyo Medical and Dental University, 1-5-45 Yushima, Bunkyo-ku, Tokyo 113-8510, Japan
[2]The Center for Brain Integration Research, Tokyo Medical and Dental University, Tokyo, Japan
Full list of author information is available at the end of the article

mice, the first animal model of normal tension glaucoma [14]. Furthermore, we recently reported that GluN2D deficiency partially protected against the loss of RGCs in GLAST KO mice [15]. These results suggest that other GluN2 subunits, in addition to GluN2D, may contribute to excitotoxic retinal cell death. To address this hypothesis, we examined the roles of the four different GluN2 subtypes in NMDA-induced retinal cell death using mice lacking specific GluN2 subunits. We also evaluated the neuroprotective effect of 7-hydroxy-6-methoxy-2-methyl-1-(2-(4-(trifluoromethyl)phenyl)ethyl)-1,2,3,4-tetrahydroisoquinoline hydrochloride (HON0001) [16], an specific GluN2B antagonist, on RGC degeneration due to glutamate excitotoxicity in GLAST KO mice.

In the present study, we report that GluN2B and GluN2D deficiency protect against NMDA-induced excitotoxic retinal cell death, but GluN2A and GluN2C deficiency have no protective effects. We also show that pharmacological blockade of GluN2B subunit attenuates RGC loss in GLAST KO mice.

Results

NMDA receptor subunits present in mouse RGCs

To investigate the expression of NMDAR subunits in RGCs, we used a single-cell reverse transcriptase polymerase chain reaction (RT-PCR) method. After dissociation of the retina into single cells, RGCs can no longer be identified by their morphology. We therefore used dissociated retina from B6.Cg-TgN(Thy1-CFP)23Jrs/J transgenic mice (thy1-CFP mice), which express cyan fluorescent protein (CFP) in most RGCs [17]. We first confirmed that the CFP-containing cells in the thy1-CFP mouse retina were RGCs by immunostaining with Brn3, a neurochemical marker for RGCs [18]. CFP expression colocalized with Brn3 immunoreactivity in most somata in the ganglion cell layer (GCL) (Figure 1A-C). A single CFP-expressing cell was picked with a glass capillary from the dissociation mix and transferred to the reaction tube (Figure 1D, E), and was further identified as RGC by expression of Brn3 (Figure 1F). Typical results of single-cell RT-PCR on isolated RGCs are shown in Figure 1F. GluN1 and GluN2A–D could be amplified together with an internal control (β-actin) from a single RGC, as well as from whole retina. In our samples of 4 isolated RGCs, two cells express GluN1/GluN2A/GluN2B/GluN2C/GluN2D, whereas the other two cells express GluN1/GluN2A/GluN2B/GluN2D. These results indicate the presence of GluN1 and all GluN2 subunits (GluN2A–D) in the mouse RGCs.

Retinal structure in mice lacking GluN2 subunits

We used mice lacking any one of the four GluN2 subunits to determine the distinct roles of these GluN2 subunits in NMDA-induced RGC death. Mice lacking GluN2A,

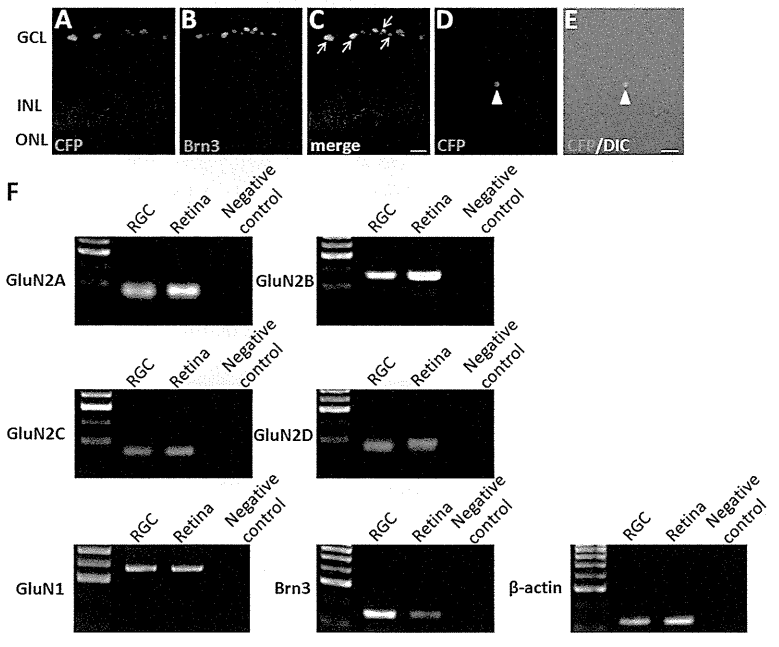

Figure 1 Expression of NMDA receptor subunits in mouse retinal ganglion cell. (A-C) Immunohistochemical analysis of Brn3 (**B** red) in Thy1-CFP mice. CFP fluorescence (**A** green) was overlaid with Brn3 **(C)**. Arrows in **(C)** indicate double-labeled cells. Scale bar, 20 μm. **(D-E)** After dissociation the fluorescent RGC was picked up from the cell suspension. CFP (green) and DIC pictures for the same isolated cell are superimposed **(E)**. Arrowhead indicates CFP-expressing RGC. Scale bar, 20 μm. **(F)** Single-cell RT-PCR analysis for GluN1, four GluN2 subunits, Brn3 and β-actin. Distilled water was used for PCR negative control. GCL, ganglion cell layer; INL, inner nuclear layer; ONL, outer nuclear layer; RGC, retinal ganglion cell.

GluN2C, and GluN2D are viable [19-21], whereas GluN2B-deficient mice die shortly after birth [22]. We therefore generated conditional GluN2B KO mice, in which GluN2B was ablated in retinal neurons containing RGCs. For this purpose, we crossed GluN2B$^{f/f}$ [23] mice with c-kit-Cre mice [24] (GluN2B$^{f/f}$/c-kit-Cre). In c-kit-Cre mice crossed with ROSA-tdTomato reporter mice [25] (ROSA-tdTomato/c-kit-Cre), tdTomato-expressing cells were localized in the GCL and inner nuclear layer (INL) and most calretinin immunoreactive cells (RGCs and amacrine cells) contained tdTomato, suggesting that Cre recombinase is expressed in RGCs and cells in the INL, including amacrine cells, in c-kit-Cre mice (Figure 2A). Immunohistochemical analysis revealed that GluN2B protein expression was eliminated in RGCs and cells in the INL in GluN2B$^{f/f}$/c-kit-Cre mice (Figure 2B). Western blot analysis showed that GluN2A, GluN2C, and GluN2D proteins were completely eliminated from mutant mice lacking GluN2A, GluN2C, and GluN2D, respectively (Figure 2C, E, F). In GluN2B$^{f/f}$/c-kit-Cre mice, GluN2B expression level in the retina was significantly lower than in control mice (Figure 2D).

We next investigated whether the absence of GluN2 subunits affects the anatomical organization of the retina by histological analyses. Hematoxylin and eosin staining revealed the retinae of GluN2A, GluN2B$^{f/f}$/c-kit-Cre, GluN2C, and GluN2D mutant mice to be normally organized, consisting of several different cell layers (Figure 3A). The thickness of the inner retinal layer (IRL) in all mutant strains was normal compared with wild-type (WT) mice (Figure 3B). As previous studies showed that ablation of GluN1 increased cell death in the developing somatosensory thalamus [26], we counted cell numbers in the GCL. The cell number in the GCL of GluN2B$^{f/f}$/c-kit-Cre mice was significantly lower than that of WT mice at 5 weeks, whereas cell number in the GCL of the other mutant strains was comparable to that of control mice at 5 weeks (Figure 3C). These results suggest that GluN2B subunit plays a survival role for RGCs during retinal development, but the other GluN2 subunits (GluN2A, GluN2C and GluN2D) are not involved in retinal development and survival in RGCs.

GluN2B and GluN2D deficiency prevents NMDA-induced-excitotoxic retinal cell death

To determine which GluN2 subtypes are involved in NMDA-induced RGC death in the retina, we examined the effect of intraocular injection of NMDA on retinal cell death in GluN2 KO and WT mice. First, to examine the acute injury of NMDA, TUNEL analysis was performed

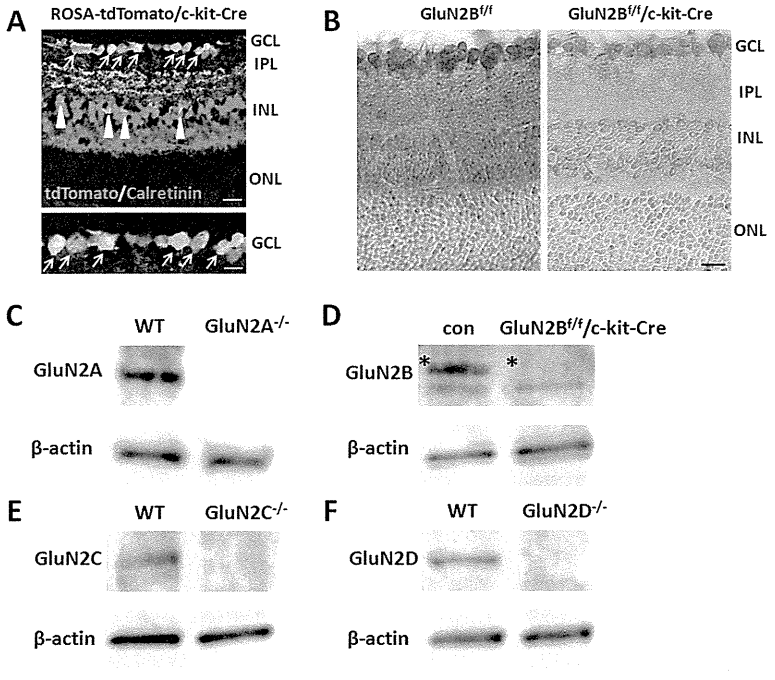

Figure 2 Ablation of GluN2 subunits in the retinas of mutant mice. (A) Immunostaining of calretinin (green) in ROSA-tdTomato/c-kit-Cre mice. Overlapping of tdTomato fluorescence (red) and calretinin indicated that Cre-mediated recombination occurs in RGCs (arrows) and amacrine cells (arrowheads). Enlarged image of the GCL in the upper panel was shown. Scale bar, 20 μm (upper) and 10 μm (lower). **(B)** Immunohistochemical analysis of GluN2B in GluN2B$^{f/f}$ and GluN2B conditional knockout mice (GluN2B$^{f/f}$/c-kit-Cre). Scale bar, 20 μm. **(C-F)** Western blot analysis of retinas from WT and GluN2 mutant mice with respective antibodies (GluN2A, GluN2B, GluN2C, GluN2D and β-actin). For GluN2B, control (con) represents GluN2B$^{f/f}$ mice. Asterisks indicate the GluN2B protein bands. Each lane was loaded with 30 μg of proteins. GCL, ganglion cell layer; IPL, inner plexiform layer; INL, inner nuclear layer; ONL, outer nuclear layer.

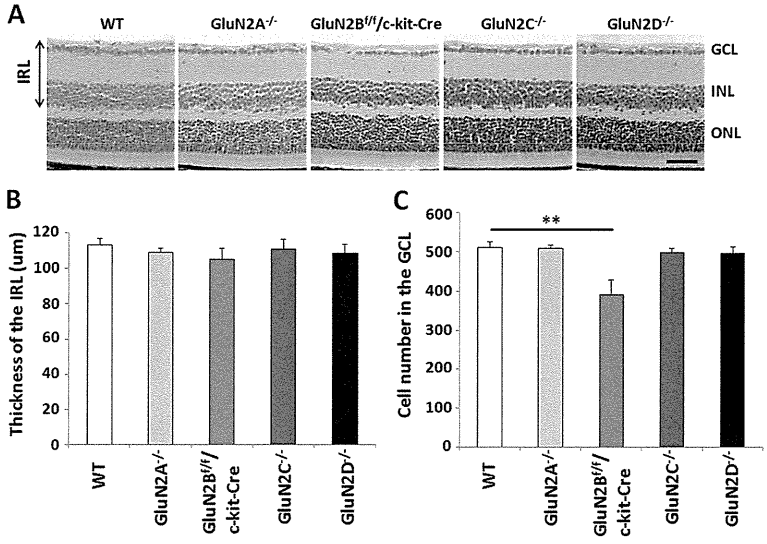

Figure 3 Effects of GluN2 subunits ablation on the morphology of the retina. (A) Hematoxylin and eosin staining (H&E) of retinal sections at P35 in WT and GluN2 mutant mice. Scale bar, 50 μm. **(B-C)** Quantification of thickness of the inner retinal layer **(B)** and the cell number in the GCL **(C)** in WT and GluN2 mutant mice. The data are presented as mean ± S.E.M. of 5 samples for each experiment. $^{**}P$ <0.01. GCL, ganglion cell layer; INL, inner nuclear layer; ONL, outer nuclear layer; IRL, inner retinal layer.

on the retinas of WT and GluN2 mutants at 1 day after NMDA treatment. A number of TUNEL-positive cells were observed in the GCL and INL in both WT and GluN2 mutant strains after NMDA injection (Figure 4A), but the percentage of TUNEL-positive cells in the GCL of GluN2B$^{f/f}$/c-kit-Cre and GluN2D$^{-/-}$ mice was significantly lower than that in WT mice (Figure 4B). Following NMDA injection, the number of RGCs and the thickness of IRL decreased from days 1 to 7, with no further decrease being observed from days 7 to 14 [27,28]. To examine the chronic injury of NMDA, morphological changes were measured 7 days after NMDA or phosphate-buffered saline (PBS) injection. Intraocular administration of NMDA induced cell death in the GCL in both WT and GluN2 mutant mice (Figure 4C), but the percentage of surviving cells in the GCL was significantly larger in GluN2B$^{f/f}$/c-kit-Cre and GluN2D$^{-/-}$ mice than in WT mice (Figure 4D). Additionally, the thickness of IRL was significantly larger in GluN2B$^{f/f}$/c-kit-Cre mice than in WT mice (Figure 4E). Taken together, these results suggest that GluN2B and GluN2D were involved in NMDA-induced RGC death.

A specific GluN2B antagonist, HON0001, prevents RGC death in GLAST-deficient mice

We have reported that the neuroprotective role of apolipoprotein E-containing lipoproteins in glaucomatous retinal degeneration in GLAST KO mice is mediated through promoting interaction between low density lipoprotein receptor-related protein 1 (LRP-1) and the GluN2B subunit [29]. Recently, we have also demonstrated that Dock3 overexpression prevented retinal cell death in GLAST KO mice by promoting GluN2B degradation [28]. To determine whether GluN2B is involved in RGC degeneration in GLAST-deficient mice, we evaluated the effect of a specific GluN2B antagonist, HON0001, on RGC degeneration in GLAST KO mice. As shown in Figure 5, the number of cells in GLAST KO mice subjected to HON0001 (10 mg/kg) treatment (281 ± 26) was significantly greater than that in GLAST KO mice not subjected to HON0001 treatment (203 ± 10). These results suggest that GluN2B is involved in RGC loss in GLAST KO mice.

Discussion

We previously reported that GluN2D deficiency prevented loss of RGCs in GLAST KO mice [15]. These results suggest that both GluN2B and GluN2D subunits play a critical role in RGC degeneration by glutamate excitotoxicity. Therefore, an GluN2B-selective antagonist in combination with an GluN2D-selective antagonist represents an effective strategy for the management of glaucoma and various forms of retinopathy. We recently showed that Dock3 overexpression prevented excitotoxic RGC death by suppressing the surface expression of GluN2D and enhancing NMDA-mediated GluN2B degradation [15,28]. Thus, the design of compounds capable of increasing the expression of Dock3 represents a novel strategy for the treatment of various forms of retinopathy. Previous studies also showed that calcium influx through NMDARs is modulated by LRP-1 [30,31]. These